Energetics of Reactions between Ceramic Coating Materials and their Binary Oxide Components with Silicate Melts

Gustavo Costa[1*], Bryan J. Harder[1], Narottam P. Bansal[1], Jamesa L. Stokes[1], Kristina Lilova[2], Tamilarasan Subranami[2], Sergey V. Ushakov[2], Kevin J. Meisner[2], Alexandra Navrotsky[2]

[1]NASA Glenn Research Center, 21000 Brookpark Road, Cleveland OH, 44135
[2] School of Molecular Sciences and Center for Materials of the Universe, Arizona State University, Tempe AZ 85281

Abstract

This paper summarizes our previous and current studies of using high-temperature calorimetry to investigate the energetics of reactions of ceramic coating materials (e.g., yttrium disilicate and 7 wt% yttria-stabilized zirconia) and their binary oxide components with silicate melts in the CaO-MgO-Al_2O_3-SiO_2 (CMAS) system. Such interactions are found to become stronger (more exothermic) with increasing difference in acid-base character between these materials and the melt. Our results suggest that the reactivity between the coating materials and the melt increases with decreasing thermodynamic stability (less exothermic enthalpy of formation from oxide components) of the coating material. They also suggest that ceramic coating materials made from binary oxides that have less exothermic enthalpies of solution and mixing are less susceptible to CMAS melt corrosion when in contact with an acidic, relatively polymerized melt rich in SiO_2. Thus, we propose that new coating material formulation and CMAS melt corrosion mitigation strategies should be optimized based on the energetic contributions of their binary oxide components.

Introduction

The desire for improved efficiencies in gas-turbine engines has driven the development of ceramic coatings to protect hot section components from elevated temperatures and corrosive combustion products.[1-10] The ceramic coatings used to provide thermal protection are known as thermal barrier coatings (TBCs),[1,3-6] and are traditionally based on zirconia (e.g., 7 wt% yttria-stabilized zirconia, 7YSZ). Coatings that are used to provide environmental protection for silicon-based ceramics are known as environmental barrier coatings (EBCs),[2,7-10] and are currently based on rare earth silicates (e.g., $Yb_2Si_2O_7$). Although both TBCs and EBCs have shown durability in engine environments, they are still susceptible to silicate melt corrosion caused by ingested particulate silicate debris which may cause failure due to thermomechanical and/or thermochemical effects[9,11,12]. The composition of the silicate debris source, which is mainly composed of CaO-MgO-Al_2O_3-SiO_2 (CMAS), directly affects corrosion reactions with the coating materials and phase equilibria with the silicate melt.[12]

The corrosiveness or reactivity of coating materials and their binary oxide components with silicate melts can be directly related to their thermodynamic properties such as enthalpies of solution, mixing and formation.[13] In addition, these properties provide the fundamental basis of understanding melt speciation such as their polymerization degree which is a direct measure of acid-base character, and interaction of their components at molecular level.[14] Such properties of ceramic coating materials and their binary oxide components can be directly measured by high temperature calorimetry using silicate melts as solvent.[13-21] Similarly, entropy for each thermodynamic term (e.g. solution and mixing) would be certainly positive and large enough to overcome the enthalpic terms resulting in a negative free energy. As discussed below, the focus of our previous[13] and this current study is to use high temperature calorimetry to measure the

enthalpic thermodynamic properties of coating materials and their binary oxide components in silicate melts for correlating them with reactivity and melt speciation since the entropy terms are not easily measured by standard calorimetric techniques.

In our previous work,[13] we measured the enthalpies of solution of relevant coating materials and calcium rare earth silicate oxyapatites (specifically, 7YSZ ($Zr_{0.88}Y_{0.12}O_{1.94}$), 31YSZ ($Zr_{0.53}Y_{0.47}O_{1.77}$), 16RESZ ($Zr_{0.73}Y_{0.172}Gd_{0.056}Yb_{0.045}O_{1.86}$), $Y_2Si_2O_7$, $Yb_2Si_2O_7$, $CaY_4Si_3O_{13}$, and $CaYb_4Si_3O_{13}$) in a silicate melt with a composition of 30CaO-5.3MgO-11.9Al_2O_3-8.7Fe_2O_3-1.5NiO-42SiO_2 (mol%), similar to deposits found on turboshaft shrouds operated in a desert environment[22]. All coating materials had moderate positive enthalpies of solution in this CMAS composition, except 7YSZ, which exhibited a negative enthalpy of solution. The enthalpies of mixing of 7YSZ, $Yb_2Si_2O_7$, and $CaYb_4Si_3O_{13}$ liquids with CMAS melt, calculated from their enthalpies of solution and of fusion, indicated higher energetic stability of $Yb_2Si_2O_7$ and $CaYb_4Si_3O_{13}$ (less exothermic or less reactive) than 7YSZ against silicate melt corrosion. From the enthalpy of mass-balanced reactions between the coating materials and molten CMAS resulting in oxyapatite formation, we found that for 7YSZ oxyapatite is only favorable to form over coating dissolution, although other crystalline phases detected by high-temperature X-ray diffraction (XRD) may complicate the energetic pathway for phases in equilibrium at high temperature.

In this work, we use high-temperature reaction calorimetry[13-21] at 1723 K to measure the enthalpies of drop solution (ΔH_{ds}) of CaO, MgO, Al_2O_3, SiO_2, Y_2O_3, Yb_2O_3, Gd_2O_3 and ZrO_2 binary oxides and $Y_2Si_2O_7$, $Yb_2Si_2O_7$, $Gd_2Zr_2O_7$ ternary oxides in CMAS melts with varying SiO_2 content. Three CMAS compositions[23-25] 30CaO-5.3MgO-11.9Al_2O_3-8.7Fe_2O_3-1.5NiO-42SiO_2, 17.7CaO-10.0MgO-7.0Al_2O_3-65.3SiO2 and 26.7CaO-9.8MgO-7.7Al_2O_3-55.8SiO_2 were used as molten solvents in the calorimetric experiments. These CMAS compositions are within the

composition range of silicate debris from different global locations[9,11,12,22,26-28] that are relevant for silicate melt corrosion of coating materials applied on the hot section of gas turbine engines. The transposed temperature drop enthalpy (ΔH_{TTD}, heat content from room temperature to the temperature of the calorimeter, 1723 K) of the $Gd_2Zr_2O_7$ sample measured in this study, those measured in the previous work[13] for $Y_2Si_2O_7$, $Yb_2Si_2O_7$, $CaY_4Si_3O_{13}$ and $CaYb_4Si_3O_{13}$, those of CaO, MgO, Al_2O_3, ZrO_2 and SiO_2 calculated using FactSage[29] software with FACT oxide database, and other values for rare earth oxides from the literature[30] were used to calculate their enthalpies of solution ($\Delta H_s = \Delta H_{ds} - \Delta H_{TTD}$). The enthalpy of fusion (ΔH_{fusion}) for $Y_2Si_2O_7$, required for the calculation of its enthalpy of mixing with the silicate melts, was measured by differential thermal analysis (DTA) above 1773 K. The enthalpies of solution and mixing of the $Y_2Si_2O_7$, $Yb_2Si_2O_7$, and $Gd_2Zr_2O_7$ coating materials in molten CMAS with varying SiO_2 mole percent (42, 55.8, and 65.3 mol %) and their binary oxide components in CMAS with 42 mol% SiO_2 are discussed in terms of their interrelated acid-base interactions and polymerization equilibria. The new thermochemical data provide experimental evidence concerning the reactivity of these materials with molten CMAS. Kinetic factors at low temperature, including heterogeneity and the microstructure of the coating materials which may hindering the approach to equilibrium, could affect the ability of the ions to diffuse and the system to come to overall disequilibrium. Such potential disequilibrium behavior may affect reactivity and thus needs to be considered in future work.

Experimental Materials and Methods

Sample preparation and characterization

Yttrium and ytterbium disilicate powders (99.9%) were acquired from Praxair. Gadolinium zirconate was obtained from Sulzer Metco. To assure phase purity, all three powders were heated in air to 1773 K at 10 K/min followed by a 10 h hold. The powders were then ball milled with cylindrical ZrO_2 milling media in ethanol for 24 h. The resulting powder sample was heated to 1573 K at 10 K/min and held for 10 h to eliminate any adsorbed ethanol and water and assure full crystallinity of the sample. Three CMAS compositions (listed in Table 1) with a varying mole fraction of SiO_2 were utilized in this study. CMAS-1 was synthesized at Washington Mills using NASA specifications. CMAS-2 and CMAS-2.5 were prepared by melting mixtures of $CaCO_3$ (>99.0%, Alfa Aesar), MgO (99.95%, Cerac Inc.), Al_2O_3 (>99.0%, Alfa Aesar), and SiO_2 (99.5%, Alfa Aesar) at 1773 K followed by quenching. Details of CMAS and coating materials preparation as well as the chemical and structural characterization are given in our previous studies.[13,23-25] CaCO3, Y_2O_3, and Yb_2O_3 (all of 99.99% purity by metals basis) were purchased from Alfa Aesar. MgO (99.99%), Al_2O_3 (99.5%), and Gd_2O_3 (99.99%) were purchased from Sigma Aldrich. ZrO_2 (laboratory grade) is from Fisher Scientific. SiO_2 was in the form of a natural quartz crystal from Herkimer, NY. It was selected for the lack of visible impurities and inclusions.

The chemical compositions of the three coating materials were measured by energy dispersive X-ray spectroscopy (EDS) using an X-Max^N energy-dispersive X-ray silicon drift detector (EDS-SSD) (Oxford Instruments, Abingdon, United Kingdom) mounted in a Tescan MAIA3 Triglav^{TM} scanning electron microscope (Brno – Kohoutovice, Czech Republic). The crystallinity and phase purity of the powders were analyzed by X-ray diffraction (XRD) on a D8 Discover diffractometer (Bruker-AXS GmbH, Karlsruhe, Germany). XRD patterns were acquired

from 10 º to 120º 2θ with a step size of 0.020º and a collection time of 2.5 s/step. The samples were rotated during data collection. Crystalline phases were identified using International Centre for Diffraction Data (ICDD) Powder Diffraction File (PDF-4+, 2019) and Jade 2010 v.3 software (Materials Data Inc, Livermore, CA).

High-temperature reaction calorimetry

Enthalpies of drop solution (ΔH_{ds}) and transposed temperature drop (ΔH_{TTD}) of the powder samples were measured in a Setaram MHTC-96 calorimeter (Caluire-et-Cuire, France). The drop solution experiment consisted of dropping pellets (~10 mg) of uniaxially pressed powder samples from room temperature into ~10 g of molten CMAS in a platinum crucible in the calorimeter at 1723 K. The transposed temperature drop experiment was performed under the same conditions but in an empty platinum crucible, providing the heat content of the sample from room temperature to temperature of the calorimeter. Measurements were repeated 5–10 times to achieve statistically reliable data. The calorimeter was calibrated against the heat content of corundum. The procedure has been described previously in detail. [13-21]

Differential thermal analysis (DTA) of yttrium disilicate

The enthalpy of fusion of yttrium disilicate was measured in a Setaram Setsys Evolution 2400 differential thermal analyzer (Caluire-et-Cuire, France) using a tungsten-rhenium sensor and vitreous carbon furnace protection tube. Temperature sensitivity calibration was performed by melting Au and Al_2O_3 standards at the same experimental conditions. The sample was heated at 1073 K for 3 h and sealed in a tungsten crucible by TIG (tungsten-inert gas) welding under argon flow. The measurements were performed on two samples, 35 and 45 mg in weight, at heating and cooling rates of 20 K/min in an argon flow of 40 mL/min. Fusion enthalpy was taken as the average

from heat effects on heating and cooling. After measurements, instrument calibration was repeated. Calibration uncertainties for measurements between 1273 and 2273 K are estimated as ±2 K in temperature and <2% in enthalpy.

Results

Chemical composition and X-ray diffraction data

The yttrium and ytterbium disilicates and CMAS samples in this study are the same as those of our previous studies and their phase purity, crystallinity, and chemical composition are given in detail in the references.[13,24] Yttrium disilicate (γ-$Y_2Si_2O_7$), ytterbium disilicate (β-$Yb_2Si_2O_7$) and gadolinium zirconate (Gd_2Zr_2O) (see supporting information for further characterization details) samples are phase pure and fully crystalline, and their chemical composition was confirmed to be the same within the analytical uncertainties as the nominal composition. Table 1 gives the details of chemical composition of the CMAS samples and their SiO_2 mole percentage. The compositions of the CMAS samples are within the range and representative of most observed silicate deposits from different global regions. [9,11,12,22,26-28] These CMAS samples are completely molten at 1553 K.[23-25] This temperature is well below the 1723 K set point of the calorimetric experiments, which results in fast and complete dissolution of the samples to record the calorimetric peaks.

High-temperature solution calorimetry and differential thermal analysis (DTA)

The enthalpies given in this work are in units of kJ/g-atom to give a consistent basis of the same number of atoms for comparison. The transposed temperature drop enthalpies ΔH_{TTD} of the EBCs, TBCs, silicate oxyapatites, and their binary oxide components are given in Table 2. Except for $Gd_2Zr_2O_7$, all TBC EBC and oxyapatite ΔH_{TTD} values are from our previous work.[13] ΔH_{TTD}

values of the binary oxides were calculated using FactSage with FACT oxide database[29] or are reference values[30.] The enthalpy of drop solution minus the enthalpy of transposed temperature drop gives the enthalpy of solution ($\Delta H_s = \Delta H_{ds} - \Delta H_{TTD}$) of the materials in molten CMAS (Table 3). ΔH_{ds} of the binary oxides were measured in this work. ΔH_{ds} of the ternary and quaternary oxides (EBCs, TBCs and oxyapatites) were taken from our previous work[13], except for $Gd_2Zr_2O_7$ measured in this work. ΔH_{ds} of 31YSZ, 16RESZ and $Y_2Si_2O_7$ were remeasured in this work. The enthalpies of drop solution of the binary oxides in 35 and 45 mol% SiO_2 CMAS melts are shown in Figure 1. The enthalpies of solution of the binary oxides in melt richer in silica are slightly exothermic except for gadolinia and calcia with moderate and high exothermic (negative) enthalpies of solution, respectively. The enthalpies of solution of calcia and magnesia become much more positive in a leaner silica CMAS melt. Alumina exhibits moderately positive enthalpy of solution in the leaner silica melt and slightly negative enthalpy of solution in the richer silica melt. The enthalpy of solution of silica is slightly more negative in the leaner silica melt than in the richer silica melt. The enthalpies of solution of silica in silicate melts with varying silica mol percentage is shown in Figure 2. Values become more negative with decreasing silica content in binary and multicomponent oxide-melt-based systems. Figure 3 shows the enthalpies of solution of the $Gd_2Zr_2O_7$, $Y_2Si_2O_7$, and $Yb_2Si_2O_7$ coating materials versus SiO_2 mole fraction in the molten CMAS. The enthalpy of solution of $Y_2Si_2O_7$ and $Yb_2Si_2O_7$ becomes less endothermic with increasing SiO_2 mole fraction in the CMAS melt. The enthalpy of solution of $Y_2Si_2O_7$ is 3.42±1.70 kJ/g-atom more exothermic (more negative) than $Yb_2Si_2O_7$ in the melt with 65.3 mol% SiO_2. The enthalpies of solution of $Y_2Si_2O_7$ and$Yb_2Si_2O_7$ are the same within the experimental uncertainties in the melts with 55.8 and 42 mol% SiO_2. The enthalpy of solution of $Gd_2Zr_2O_7$ becomes slightly more endothermic with increasing SiO_2 mole fraction in the CMAS melt, and it is much more

exothermic (~10–19 kJ/g-atom) than values for $Y_2Si_2O_7$ and $Yb_2Si_2O_7$ in the composition range of this study.

The enthalpy of fusion of $Y_2Si_2O_7$ measured by DTA as an average of 12 calorimetric peaks recorded during heating and cooling segments is 151 ±1 4 kJ/mol or 13.73 ± 1.27 kJ/g-atom. The melting temperature of $Y_2Si_2O_7$ calculated from an average of the onsets of six melting peaks is 2071 ± 3 K. The uncertainties for the enthalpy of fusion and melting temperature are reported as two standard deviations of the mean. The enthalpies of fusion for $Y_2Si_2O_7$ from this study, for $CaYb_4Si_3O_{13}$, for other coating materials from our previous study,[13] and their binary oxide components[29,31-35] are given in Table 4.

These enthalpies of fusion are used to calculate the enthalpies of mixing as $\Delta H_{mix} = \Delta H_s - \Delta H_{fusion}$ between molten CMAS, the coating materials, $CaYb_4Si_3O_{13}$, and their binary oxide components. The enthalpies of mixing and fusion are deconvoluted from the enthalpy of solution and refer to mixing between supercooled liquid coating materials and the CMAS melts. The enthalpies of mixing between the coating materials and their binary oxide components and silicate melts with varying mol % SiO_2 from Table 5 are shown in Figures 4–6. As expected, the enthalpy of mixing of coating materials, $CaYb_4Si_3O_{13}$, and their binary oxide components, which have the energetic contribution from the enthalpy of fusion are more negative and follow the same trend of their enthalpies of solution shown in Figures 1–3.

The enthalpies of formation of the coating materials at 298 K calculated from the enthalpies of drop solution of binary oxide components in CMAS are given in Table 6. The thermochemical cycles and details of the enthalpy of formation calculations are given in the supporting information. The enthalpies of formation calculated from the drop solution measurements of this work are in

good agreement to those measured or calculated previously[13, 36-41] using different methodologies and solvents.

Discussion

To understand the reactivity and thermodynamic properties involving silicate melts (e.g., molten CMAS) and coating materials, it is necessary to depict the structure of these melts and establish the mechanisms of interactions between the silicate melt structure and other cations (modifiers), especially highly charged cations (Y^{3+}, Yb^{3+}, Gd^{3+}, and Zr^{4+}) from the coating materials. Silicate melts can be envisioned as ionic polymers in which SiO_4 and AlO_4 tetrahedra link to form the network.[42–44] Al_2O_3, being potentially amphoteric, can be either a network former or modifier, but at these melt compositions it is predominantly a network former.[45] Ferric iron Fe^{3+} occurs both as a network former and a modifier, and ferrous iron Fe^{2+} is a modifier.[45] The polymerization model proposed by Hess[42–43]describes the formation of a silicate melt as a reaction between liquid metal oxide and liquid silica by the homogenous equilibrium

$$Si–O–Si + M–O–M = 2Si–O–M \quad (1)$$

where M is a metal cation other then Si^{4+} and Al^{3+}. These equilibria can be written using the notation

$$O^0 + O^{2-} = 2O^- \quad (2)$$

where O^0, O^{2-} and O^- are bridging (BO), free (O), and non-bridging oxygens (NBO), respectively. This model was later reformulated by Virgo et al.,[46]who used stoichiometric notations to describe the coexisting species or structural units in the silicate melt by the anionic equilibria:

$$Si_2O_7^{6-} = SiO_4^{4-} + SiO_3^{2-} \quad (3)$$

$$2SiO_3^{2-} = SiO_4^{4-} + Si_2O_5^{2-} \quad (4)$$

$$Si_2O_5^{2-} = SiO_3^{2-} + SiO_2 \quad (5)$$

These anionic equilibria can be reduced to one equation by using the following Q^n notation:[47–50]

$$2Q^n = Q^{n-1} + Q^{n+1} \quad (6)$$

where Q is the structural element (tetrahedrally coordinated Si^{4+}, Al^{3+}, or Fe^{3+}) having an average *n* of bridging oxygens. Using the Q^n notation above, the equilibria for CMAS melts can be written as

$$2Q^3 = Q^2 + Q^4 \quad (7)$$

$$2Q^2 = Q^1 + Q^3 \quad (8)$$

$$2Q^1 = Q^0 + Q^2 \quad (9)$$

In general, the polymerization degree of the silicate melt increases by the formation of bridging oxygens (Q^n increases) with increasing network former content (SiO_2, Al_2O_3, or, in some cases, Fe_2O_3) or decreasing modifier (CaO, MgO, NiO, FeO, or, in some cases, Al_2O_3) content. Increasing polymerization degree of the melt also increases its acidity. The estimated speciation of the slag of the previous study and the three other CMAS compositions is given in Table 7. The CMAS melt (35.2 mol% SiO_2) of the previous study with mean Q^2 speciation is considered more depolymerized[21], or less acidic, than the other three CMAS compositions with speciation between Q^3 and Q^4. Thus, equilibria in equations (7) and (8) would be more prevalent for the slag (Q^2) and the three other CMAS compositions (Q^3-Q^4).

Using the equilibria above, the processes involving the interaction of coating materials and silicate melts can be addressed. Acid-base interactions, network substitution of silicon and aluminum, and the mixing of modifier ions are usually the competing processes taking place when

the coating materials react with the silicate melts.[51] The acid-base reaction[14] between coating materials and silicate melts is driven by the equilibrium

$$\text{Acid} + O^{2-} = \text{Base} \qquad (10)$$

Two equilibria can be considered for the slag melt of the previous study and the melts of this study. For relatively depolymerized slag melt with average Q^2 speciation the equilibrium can be considered to be

$$SiO_3^{2-} + O^{2-} = SiO_4^{2-} \quad (11)$$

The equilibria for relatively polymerized melts with speciation between Q^3 and Q^4 can be considered to be

$$Si_2O_5^{2-} + O^{2-} = Si_2O_7^{2-} \quad (12)$$

These reactions become more exothermic as the difference in acid-base character between the coating material or their binary oxide components and silicate melts increases.[51] The binary oxides with greater basicity or stronger interaction with the melts are expected to exhibit more exothermic (more negative) enthalpies of solution and mixing. A short discussion is provided below on the relations among energetics, oxide ion speciation, composition and melt structure although the detailed distribution of cations and oxygens (e.g., bridging, and non-bridging oxygens) in the melts of this study is not known in detail.

Taking the reactions between the silicate melts and oxide ions shown above (1, 10-12), it is expected that an oxide ion from a more basic binary oxide would interact more strongly with the silicate species in the melt, resulting in more exothermic (negative) enthalpies of solution and mixing. This effect is evident in the more exothermic enthalpies of solution and mixing of CaO

compared to MgO shown in Figures 1 and 4, and Tables 3 and 5 and reflects the greater basicity of CaO than of MgO.

The higher exothermicity of CaO and MgO dissolution in more SiO_2 rich melts is related to the melt equilibrium environment (Figures 1 and 4, and Tables 3 and 5). Oxygen ions from CaO and MgO would see an environment with more bridging oxygens in more SiO_2 rich melts. The initial formation of nonbridging oxygens would be more exothermic in the more polymerized, silica-rich, and more acidic melts. This increasing exothermicity in dissolution enthalpy of basic oxides with increasing silica content reflects increasing thermodynamic activity of silica in the more polymerized melts, and its sharper decrease with addition of basic oxide solute which decreases the degree of polymerization of the melt.

As **s**ilica is added to a silicate melt, it reacts with non-bridging oxygens (NBO) to form bridging oxygens (BO). As BO increases, the melt becomes more polymerized or acidic (Q^n increases). As discussed above, it would be expected that the interaction between acidic silica (Q^4) and the melt would become stronger with increasing basicity or decreasing polymerization of the melt (Q^n). Figures 2 and 5 show that the interaction of acidic silica and the melt becomes more exothermic with decreasing SiO_2 content and decreasing polymerization. That is, the less polymerized or more basic the melt is, the stronger and more exothermic its interaction with acidic silica.

To a good approximation, the NBO in aluminosilicate glasses and melts, if present, will be converted to BO when alumina is added, meaning that Al^{3+} is a network former mainly present as AlO_4. tetrahedra[50] All NBO will be converted to BO and the melt is entirely connected by tetrahedra when the alumina content becomes great enough to balance all modifier oxides.[50] Especially at higher alumina contents when there are not enough mono and divalent cations to

charge balance the tetrahedral aluminum, spectroscopic studies of calcium aluminosilicates indicates that AlO_5 and AlO_6 groups can be present in some glass-forming regions, confirming that Al^{3+} also acts as a modifier.[52] However this is not the case for the compositions studied here. The more negative enthalpies of solution and mixing of alumina in the more silica rich melt (Figures 1 and 4, and Tables 3 and 5) suggest that Al^{3+} exhibits a network modifier character in the more polymerized melts.

Rare earth cations and zirconium in glasses and silicate melts are generally considered to bond (coordinate) to non-bridging oxygens and oxygens from modifiers (e.g. Ca, Mg) rather than entering the network because of their large size and high coordination (≥ 6). [53-55] These cations are expected to form clusters containing free oxide ions isolated from the silicate network. The more exothermic enthalpies of solution and mixing of Gd_2O_3 than Y_2O_3 Yb_2O_3 and ZrO_2 suggest that gadolinium is more effective in competing with the other rare earths and zirconium for oxygen in the silicate melt. This higher exothermicity also reflects the greater basicity and interaction of Gd_2O_3 with the melt (Figures 1 and 4, and Tables 3 and 5).

Coating materials

The energetics of reaction of the coating materials can be directly correlated to the enthalpic contribution of their binary oxide components. This correlation agrees with those observed for the enthalpies of solution and mixing of EBCs ($Yb_2Si_2O_7$ and $Y_2Si_2O_7$), TBCs (7YSZ, 31YSZ, and 16RESZ) and oxyapatites ($CaY_4Si_3O_{13}$ and $CaYb_4Si_3O_{13}$), which take the enthalpic contribution from their binary oxide components (Tables 3 and 5, and Figures 1–6). The rare earth zirconia-based coating materials react more exothermically than the silicate-based coatings and oxyapatites, reflecting the higher exothermic contribution of their binary oxide components. The silicate coatings and oxyapatites show lower exothermicity of reaction with the 42 mol% SiO_2 CMAS

melt when compared to pure silica, reflecting their weak interaction with the melt. This indicates a small difference between the acid-base character between their components (Y_2O_3, Yb_2O_3, CaO, and the silicate $Si_2O_7^{6-}$ and SiO_4^{2-} groups) and the melt when compared to pure silica. This weaker energetic interaction suggests that the most dominant species in the melt are the silicate groups $Si_2O_7^{6-}$ (Q^1) and SiO_4^{2-} (Q^0) in coating disilicate and oxyapatite when compared to the group SiO_2 (Q^0) in silica and that the reactivity in this melt should increase with increasing BO (Q^n) in the coating material. The small dependence of the enthalpy of solution (a measure of reactivity) of the disilicates versus melt composition results from the endothermic contribution of acidic silica energetically balancing the exothermic contribution from yttria and ytterbia as the melt becomes more polymerized. The higher stability of disilicates as solids (more exothermic enthalpies of formation) results in their lower reactivity with the melt (more endothermic heats of solution and mixing) when compared to gadolinium zirconate.

The above interactions provide important insights to their reactivity based on the CMAS source and form. As a rule, we propose that the energetic contribution of binary oxides to the reactivity of coating materials with CMAS melts is the dominant term that should be considered in CMAS-induced corrosion mitigation strategies and coating formulation.

Conclusions

The energetic interactions between the coating materials (7YSZ, 31YSZ, 16RESZ, $Gd_2Zr_2O_7$, $Y_2Si_2O_7$, and $Yb_2Si_2O_7$), apatites ($CaY_4Si_3O_{13}$ and $CaYb_4Si_3O_{13}$), their binary oxide components and molten CMAS with varying mol% SiO_2 have been measured directly by high-temperature solution calorimetry. The exothermicity of reaction between coating material or their binary oxide components and the CMAS melt reflects the difference between their acid-base character. The reactivity of coating materials and their binary oxides with CMAS melts increases

with increasing difference in their acid-base character. Thus, coating materials formulated from binary oxides with less exothermic enthalpies of solution and mixing are predicted to be less reactive or susceptible to CMAS corrosion. Furthermore, the reactivity between the coating materials and the melt is expected to increase with decreasing stability of the coating as a solid or as the coating's enthalpy of formation becomes less exothermic.

Acknowledgments. This work was supported by NASA's Transformative Tools and Technologies (TTT) Project within the Transformative Aeronautics Concept Program. We are thankful to Prof. Jonathan Stebbins for helpful discussions.

References

1. Padture NP. Advanced structural ceramics in aerospace propulsion. Nat Mater. 2016;15:804-809.

2. Padture NP. Environmental degradation of high-temperature protective coatings for ceramic-matrix composites in gas-turbines. Npj Mater Degrad. 2019;11:1-6.

3. Spitsberg I, Steibel J. Thermal and environmental barrier coatings for SiC/SiC CMCs in aircraft engine applications. Int J Appl Ceram Technol. 2004;1:291-301.

4. Padture NP, Gell M, Jordan EH. Thermal barrier coatings for gas-turbine applications. Science. 2002;296:280-284.

5. Evans AG, Clarke DR, Levi CG. The influence of oxides on the performance of advanced gas turbines. J Eur Ceram Soc. 2008;28:1405-1419.

6. Clarke DR, Oechsner M, Padture NP. Thermal-barrier coatings for more efficient gas-turbine engines. MRS Bull. 2012;37:891-898.

7. Lee, KN. Environmental barrier coatings for SiCf/SiC. In: Bansal NP, Lamon J, editors. Ceramic materials and composites: Materials modeling and technology. Hoboken, New Jersey: Wiley, 2015; p. 430-451.

8. Lee KN, Fox DS, Bansal NP. Rare earth silicate environmental barrier coatings for SiC/SiC composites and Si3N4 ceramics. J Eur Ceram Soc. 2005;25:1705-1715.

9. Tejero-Martin D, Bennett C, Hussain Tanvir. A review on environmental barrier coatings: History, current state of the art and future developments. J Eur Ceram Soc. 2021;41:1747-1768.

10. Gardier G. Aeroengine composites, pat 1: The CMC invasion. Compos World. Cincinnati, OH. Gardner Business Media, Inc.; 2015.

11. Poerschke DL, Jackson RW, Levi CG. Silicate deposit degradation of engineered coatings in gas turbines: Progress toward models and materials solutions. Annu Rev Mater Res. 2017;47:16.1-16.34.

12. Ericks AR, Zok FW, Poerschke DL, Levi CG. Protocol for selecting exemplary silicate deposit compositions for evaluating thermal and environmental barrier coatings. J Amer Ceram Soc. 2022;105:3665-3688.

13. Costa GC, Harder BJ, Wiesner VL, et al. Thermodynamics of reaction between gas-turbine ceramic coatings and ingested CMAS corrodents. J Am Ceram Soc. 2019;102:2948-2964.

14. Navrotsky A. Energetics of silicate melts. In: Stebbins JF, McMillan PF, Ding-well DB, editors. Structure, dynamics and properties of silicate melts. Rev Miner Geochem. 1995;32:121-143.

15. Gan H, Wilding MC, Navrotsky A. Ti^{4+} in silicate melts: Energetics from high -temperature calorimetric studies and implications for melt structure. Geochim Cosmochim Acta. 1996;60:4123-4131.

16. Wilding MC, Navrotsky A. The dissolution of silica and alumina in silicate melts: In situ high temperature calorimetric studies. Neues Jahrbuch für Mineralogie. Rosenhauer Memorial. 1998;172:177-201.

17. Wilding MC, Navrotsky A. High temperature calorimetric studies of the heat of solution of La_2O_3 in silicate liquids. J Non Cryst Solids. 2000; 265: 238-251.

18. Morishita M, Navrotsky A, Wilding MC. Direct measurement of relative partial molar enthalpy of SiO_2 in $SiO_2 – M_2O$ (M=Li, Na, K, Cs) binary and $SiO_2 – CaO – Al_2O_3$ ternary melts. J Am Ceram Soc. 2004;87:1550-1555.

19. Morcos RM, Ellis BG, Navrotsky A. The energetics of hematite dissolution in iron oxide rich melts: In situ high temperature calorimetric studies. Am Min. 2007; 92: 1064-1070.

20. Morcos RM, Navrotsky A. Iron ore sintering: characterization by calorimetry and thermal analysis. J Therm Anal Calorim. 2009;96:353-341.

21. Koryttseva A, Navorstky A. High-temperature calorimetric study of oxide component dissolution in a $CaO-MgO-Al_2O_3-SiO_2$ slag at 1450 ºC, J Amer Ceram Soc. 2017; 100: 1172-1177.

22. Borom MP, Johnson CA, Peluso LA. Role of environmental deposits and operating surface temperature in spallation of air plasma sprayed thermal barrier coatings. Surf Coat Technol. 1996; 86–87:116-126.

23. Costa, GCC, Zhu D, Kulis MJ, Acosta W. Reactivity between rare-earth oxides based thermal barrier coatings and a silicate melt. J Amer Ceram Soc. 2018;101:3674-3693.

24. Stokes JL, Harder BJ, Wiesner VL, et al. High-temperature thermochemical interactions of molten silicates with $Yb_2Si_2O_7$ and $Y_2Si_2O_7$ environmental barrier coating materials. J Eur Ceram Soc. 2019;39:5059-5067.

25. Stokes JL, Harder BJ, Wiesner VL, et al. Effects of crystal structure and cation size on molten silicate reactivity with environmental barrier coating materials. J Am Ceram Soc. 2020;103:622-634.

26. Smialek JL, Archer FA, Garlick RG. Turbine airfoil degradationin the Persian Gulf war. JOM. 1994;46(12):39–41.

27. Krueger BJ, Grassian VH, Cowin, JP, et al. Heterogeneous chemistry of individual mineral dust particles from different dust sources regions: the importance of particle mineralogy, Atmos Environ. 2004;38:6253-6261.

28. Song WJ, Lavallee Y, Hess KU, et al. Volcanic ash melting under conditions relevant to ash turbine interactions. Nat Commun. 2016;7:1-10.

29. Bale CW, Bélisle E, Chartrand P, et al. FactSage thermochemical software and databases, 2010-2016. CALPHAD. 2016;54:35-53.

30. Zhang Y, Jung I. Critical evaluation of thermodynamic properties of rare earth sesquioxides (RE = La, Ce, Pr, Nd, Pm, Sm, Eu, Gd, Tb, Dy, Ho, Er, Tm, Yb, Lu, Sc and Y). CALPHAD. 2017;58:169-203.

31. Ushakov S, Shvarev, A, Alexeev, T, et al. Drop-and-catch (DnC) calorimetry using aerodynamic levitation and laser heating. J Amer Ceram Soc. 2017;100:754-760.

32. Kapush D, Ushakov S, Navrotsky A, et al. A combined experimental and theoretical study of enthalpy of phase transition and fusion of yttria above 2000°C using “drop-n-catch” calorimetry and first-principles calculation. Acta Mater. 2017;124:204–209.

33. Fyhrie M, Hong Q-J, Kapush D, et al. Energetics of melting of Yb_2O_3 and Lu_2O_3 from Drop and Catch Calorimetry and First Principles Computations, J Chem Thermo. 2019;132:405-410.

34. Konings, RJM, Benes O, Kovacs A, et al. The Thermodynamic Properties of the f-Elements and their Compounds. Part 2. The Lanthanide and Actinide Oxides. J Phys Chem Ref Data. 2014;43:0131-1.

35. Hong Q-J, Ushakov SV, Kapush D, et al. Combined computational and experimental investigation of high temperature thermodynamics and structure of cubic ZrO_2 and HfO_2. Sci Rep. 2018;8:14692.

36. Costa GCC, Ushakov SV, Castro RHR, Navrotsky A, Muccillo R. Calorimetric measurement of surface and interface enthalpies of yttria-stabilized zirconia. Chem Mater. 2010;22:2937-2945.

37. Cordfunke EHP, Booij AS, van der Laan RR. The thermochemical properties of Y2Si2O7 and Dy2Si2O7. J. Chem. Thermodyn 1998;30:199-205.

38. Bodenschatz C.DFT calculated data; 2021.NASA Glenn Research Center (Unpublished).

39. Fabrichnaya O, Sierfert HJ, Weiland R, Ludwing T, Aldinger F, Navrotsky A, Phase equilibria and thermodynamics in the Y2O3-Al2O3-SiO2 system, Z Metallkd. 2001;92:1083-1097.

40. Jafar M, Phapale SB, Mandal BP, Roy M, Achary SN, Mishra R, Tyagi AK. Effect of temperature on phase evolution in Gd2Zr2O7: A potential matrix for nuclear waste immobilization. J Alloys Compd 2021;867:159032.

41. Helean KB, Begg BD, Navrotsky A, Ebbinghaus B, Weber WJ, Ewing RC. Enthalpies of Formation of Gd2(Ti2-xZrx)O7 Pyrochlores. MRS Online Proceedings Library 2000;663:691.

42. Hess PC. Thermodynamic mixing properties and the structure of silicate melts. In: Stebbins JF, McMillan PF, Ding-well DB, editors. Structure, dynamics and properties of silicate melts. Rev Mineral Geochem. 1995;32;17-189.

43 Hess PC. Polymer model of silicate melts. Geochim Cosmochim Acta. 1971;35:289-306.

44. Hess PC. In: Hargraves RB, editor. Physics of magmatic processes. Princeton, NJ. Princeton University; 1980.

45. Mysen BO. Structure and properties of silicate melts. Development in Geochemistry. New York: Elsevier; 1988.

46. Virgo D, Mysen BO, Kushiro I. Anionic constitution of 1-atmosphere silicate melts: implications of the structure of igneous melts. Science. 1980;208:1371-1373.

47. Stebbins JF. Identification of multiple structural species in silicate glasses by ^{29}Si NMR. Nature. 1987;330:465-467.

48. Stebbins JF, Murdoch JB, Schneider E, et al. A high-temperature high-resolution NMR study of ^{23}Na, ^{27}Al and ^{29}Si in molten silicates. Nature. 1985;314:250-252.

49. Stebbins JF, Henderson. The Short-Range Order (SRO) and Structure. Rev Mineral Geochem. 2020;86:2-42.

50. Stebbins JF. Short-range structure and order in oxide glasses. In: Encyclopedia of Glass Science, Technology, History, and Culture. Wiley. 2021.

51. Navrotsky A. Physics and Chemistry of Earth Materials. Cambridge, UK: Cambridge University Press; 1995.

52. Neuville DR, Cormier L, Massiot D. Al coordination and speciation in calcium aluminosilicate glasses: Effects of composition determined by ^{27}Al MQ-MAS NMR and Raman spectroscopy. Chem Geol. 2006;229:173-185.

53. Wang J, Brocklesby WS, Lincoln et al. Local structures of rare-earth ions in glasses: the ‘crystal-chemistry’ approach. J Non Cryst Solids. 1993; 163: 261-267.

54. Shelby JE, Kohli JT. Rare-earth aluminosilicate glasses. J Amer Ceram Soc. 1990;73:39-42.

55. Francois Farges. Does Zr-F “complexation” occur in magmas? Chem Geol. 1996;127:253-268.

56. Zhang Y, Navrotsky A. Thermochemistry of rare-earth aluminate and aluminosilicate glasses. J Non Cryst Solids. 2004; 341: 141-151.

Table 1 – Chemical composition of the CMAS samples used as molten solvent in the high-temperature calorimetry from the literature as indicated.

CMAS	Composition (mol%)			
	SiO_2	**CaO**	**MgO**	**Al_2O_3**
Slag[21]	35.1	45.9	10.7	8.3
1*,[13,23]	42	30	5.3	11.9
2[24,25]	55.8	26.7	9.8	7.7
2.5[24,25]	65.3	17.7	10.0	7.0

*Contains 8.7 mol% Fe_2O_3 and 1.5 mol% NiO. Designed by NASA to be similar to that deposited on turboshaft shrouds operated in a desert environment, and it is referred here as CMAS-1.

Table 2 – Transposed temperature drop enthalpies of binary oxides, ternary oxides (EBCs and TBCs), and quaternary oxides (yttrium and ytterbium silicate oxyapatites).

Material	**ΔH_{TTD}***	
	(kJ/mol)	**(kJ/g-atom)**
CaO	74.49±3.72[29]	37.25±1.86
MgO	70.88±3.54[29]	35.44±1.77
Al_2O_3	171.94±8.60[29]	34.39±1.72
SiO_2	99.7±4.99[29]	33.23±1.66
Y_2O_3	178.43±8.92[30]	35.69±1.78
Yb_2O_3	187.62±9.38[30]	37.52±1.88
Gd_2O_3	180.77±9.04[30]	36.15±1.81
ZrO_2	111.23±5.56[29]	37.08±1.85
7YSZ	107.84±2.72[13]	36.64±0.92
16RESZ	106.96±2.84[13]	37.23±0.99
31YSZ	88.95±3.77[13]	32.11±1.36
$Gd_2Zr_2O_7$	440.54±3.80	40.05±0.35
$Y_2Si_2O_7$	326.74±15.05[13]	29.70±1.37
$Yb_2Si_2O_7$	318.58±4.69[13]	28.96±0.43
$CaY_4Si_3O_{13}$	539.74±14.23[13]	25.70±0.68
$CaYb_4Si_3O_{13}$	526.88±12.90[13]	25.09±0.61

*****Binary oxides TTD error assumed as 5%.

Table 3- Enthalpies of drop solution and solution of the coating materials, oxyapatites and their binary oxide components measured by high temperature calorimetry in molten CMAS at 1723 K.

SiO_2 (mol%)	Material	ΔH_{ds}* (kJ/mol)	ΔH_{ds} * (kJ/g-atom)	ΔH_s* (kJ/mol)	ΔH_s* (kJ/g-atom)
42	CaO	–110.99±3.80	–55.50±1.90	–185.48±5.50	–92.74±2.66
	MgO	68.81±2.54	34.41±1.27	–2.07±4.36	–1.04±2.18
	Al_2O_3	136.19±3.05	27.24±0.61	–35.75±9.12	–7.15±1.82
	SiO_2	87.17±4.02	29.06±1.34	–12.53±6.40	–4.18±2.13
	Y_2O_3	169.35±6.32	33.87±1.26	–9.08±10.93	–1.82±2.19
	Yb_2O_3	190.03±9.63	38.01±1.93	2.41±13.44	0.48±2.69
	Gd_2O_3	120.41±5.84	24.08±1.17	–60.36±10.76	–12.07±2.15
	ZrO_2	99.09±2.63	33.03±0.88	–12.14±6.15	–4.05±2.05
	7YSZ†	93.77±1.96[13]	31.86±0.67	–14.07±3.35	–4.78±1.14
	16RESZ†	94.28±2.65**	32.82±0.92	–12.68±3.88	–4.41±1.35
	31YSZ†	91.29±5.18**	32.96±1.87	2.34±6.41	0.84±2.31
	$Gd_2Zr_2O_7$	357.07±6.08	32.46±0.55	–83.47±7.17	–7.59±0.65
	$Y_2Si_2O_7$	453.94±10.57**	41.27±0.96	127.20±18.39	11.56±1.67
	$Yb_2Si_2O_7$	454.80±5.37[13]	41.35±0.49	136.22±7.13	12.38±0.65
	$CaY_4Si_3O_{13}$	640.22±15.52[13]	30.49±0.74	100.48±21.06	4.78±1.00
	$CaYb_4Si_3O_{13}$	769.86±7.83[13]	36.66±0.37	242.98±15.09	11.57±0.72
55.8	$Gd_2Zr_2O_7$	392.71±10.90	35.70±0.99	–47.83±11.54	–4.35±1.05
	$Y_2Si_2O_7$	414.50±10.87	37.68±0.99	87.76±18.56	7.98±1.69
	$Yb_2Si_2O_7$	444.52±19.11	40.41±1.74	125.94±19.67	11.45±1.79
65.3	$Gd_2Zr_2O_7$	392.14±3.96	35.65±0.36	-48.40±5.49	–4.40±0.50
	$Y_2Si_2O_7$	387.29±8.75	35.21±0.80	60.55±17.41	5.50±1.58
	$Yb_2Si_2O_7$	416.72±5.03	37.88±0.46	98.14±6.88	8.92±0.63

*Uncertainties are calculated as two standard deviations of the mean. Extra digit is retained to prevent-round off error. †7YSZ ($Zr_{0.88}Y_{0.12}O_{1.94}$), 31YSZ ($Zr_{0.53}Y_{0.47}O_{1.77}$), 16RESZ ($Zr_{0.73}Y_{0.172}Gd_{0.056}Yb_{0.045}O_{1.86}$). **Remeasured in this work.

Table 4- Enthalpies of fusion of the coating materials and their binary oxide components.

Material	**ΔH_{fusion} (kJ/mol)**	**ΔH_{fusion} (kJ/g-atom)**
CaO^{*}	79.50±3.97[29]	39.75±1.99
MgO^{*}	71.45±3.57[29]	35.73±1.79
Al_2O_3	120±10[31]	24.00±2.00
SiO_2^{*}	9.70±0.48[29]	3.23±0.16
Y_2O_3	119±10[32]	23.80±2.00
Yb_2O_3	102±10[33]	20.40±2.00
Gd_2O_3	92±10[34]	18.40±2.0
ZrO_2	55±7[35]	18.33±2.33
7YSZ	58±9[13]	19.73±3.06
$CaYb_4Si_3O_{13}$	240±11[13]	11.43±0.52
$Y_2Si_2O_7$	151±14	13.73±1.27
$Yb_2Si_2O_7$	151±8[13]	13.73±0.73

*****Binary oxides enthalpies of fusion error assumed as 5%.

Table 5- Enthalpies of mixing of the coating materials and their binary oxide components with molten CMAS at 1573 K.

SiO_2 (mol%)	Material	ΔH_{mix}* (kJ/mol)	ΔH_{mix}* (kJ/g-atom)
	CaO	–264.98±6.64	–132.49±3.32
	MgO	–73.52±5.64	–36.76±2.82
42	Al_2O_3	–155.75±13.54	–31.15±2.71
	SiO_2	–22.23±6.42	–7.41±2.14
	Y_2O_3	–128.08±14.82	–25.62±2.96
	Yb_2O_3	–99.59±16.76	–19.92±3.35
	Gd_2O_3	–152.36±14.69	–30.47±2.94
	ZrO_2	–67.14±9.32	–22.38±3.11
	7YSZ	–72.02±9.60	–24.51±3.27
	$CaYb_4Si_3O_{13}$	2.98±18.67	0.14±0.89
	$Y_2Si_2O_7$	–23.80±23.11	–2.16±2.10
	$Yb_2Si_2O_7$	–14.78±10.72	–1.34±0.97
55.8	$Y_2Si_2O_7$	–63.24±23.25	–5.75±2.11
	$Yb_2Si_2O_7$	–25.06±21.24	–2.28±1.93
	$Y_2Si_2O_7$	–90.45±14.61	–8.22±2.03
65.3	$Yb_2Si_2O_7$	–52.86±8.42	–4.81±0.96

*Uncertainties propagated from ΔH_s and ΔH_{fusion}.

Table 6- Enthalpies of formation (ΔH_f) of the coating materials from oxides at 298 K from this study compared with the literature.

Material	**ΔH_f (kJ/mol)**		
	This study, CMAS -1	**From literature**	
			Solvent/method
7YSZ	3.59±3.06	4.77±3.18	Sodium molybdate[36]
31YSZ	1.02±5.86	–6.92±0.70	Sodium molybdate[36]
16RESZ	18.20±3.47	----	----
$Y_2Si_2O_7$	–110.25±14.71	–91.60±4.60	Acid calorimetry, HF[37]
		–112.16	Density Functional Theory, DFT[38]
		–67.08±5.98	Alkali borate[39]
$Gd_2Zr_2O_7$	–38.48±9.93	–41.80±1.50	Sodium molybdate[40]
		–52.20±1.50	Sodium molybdate[41]

Table 7 – Estimated concentration of non-bridging and average bridging oxygens (NBO and Q^n) from CMAS compositions.

CMAS	Mol%						
	T*	**Total modifier oxides****	**Mod-ex†**	**NBO‡**	**NBO/T**	**Q^n**	**NBO/Si**
Slag	51.7	56.6	48.3	96.6	1.87	2.13	2.75
1	76.44	40.18	22.96	45.92	0.60	3.40	1.09
2	71.2	36.5	28.8	57.6	0.81	3.19	1.03
2.5	79.3	27.7	20.7	41.4	0.52	3.48	0.63

*T is the number of tetrahedral cations in 100 mol of CMAS formula. **Total modifier oxides is the sum of modifiers (e.g. CaO, MgO, FeO and NiO). †Mod-ex or modifier excess is the "excess" modifier left after "formation" of aluminate or aluminum-ferrate species (e.g., $CaAl_2O_4$, $MgAl_2O_4$ or $Ca(Al,Fe)_2O_4$, and $Mg(Al,Fe)_2O_4$). ‡Non-bridging oxygen is calculated as NBO = 2 × Mod-ex because each oxygen in the modifier oxide "reacts" with a bridging oxygen (BO) in silica to form 2 non-bridging oxygens (NBO) (O^{2-} + BO = 2NBO).

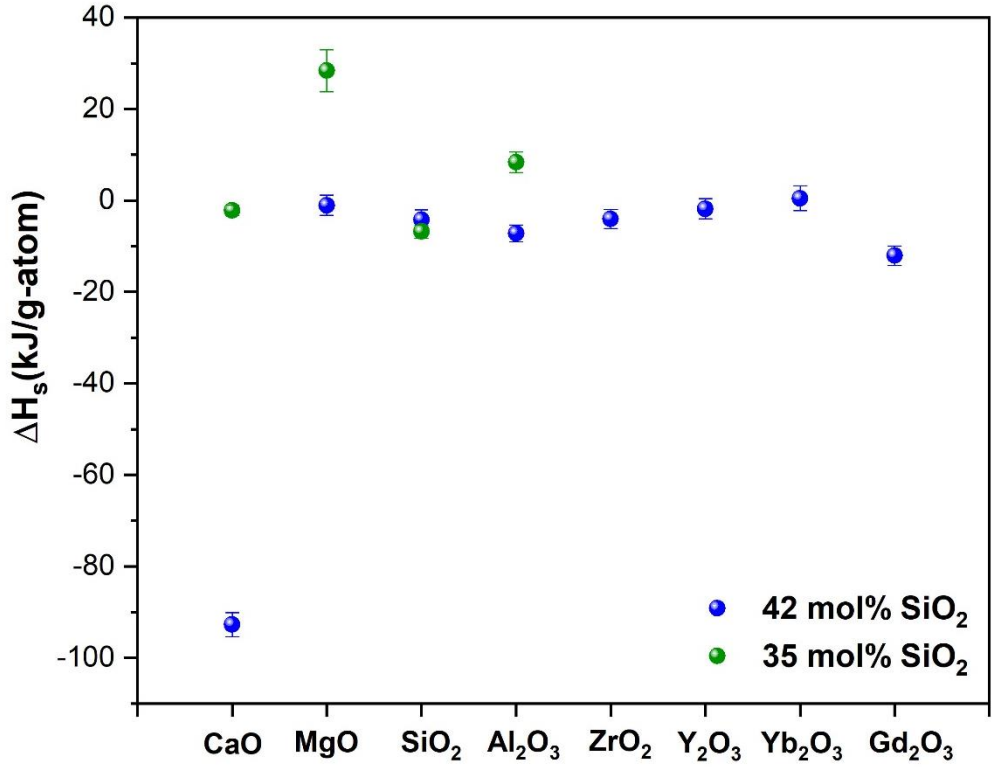

Fig. 1 – Enthalpies of solution (ΔH_s) of binary oxides in CMAS melts with 35[21] and 42 mol% SiO_2 (green and blue spheres, respectively).

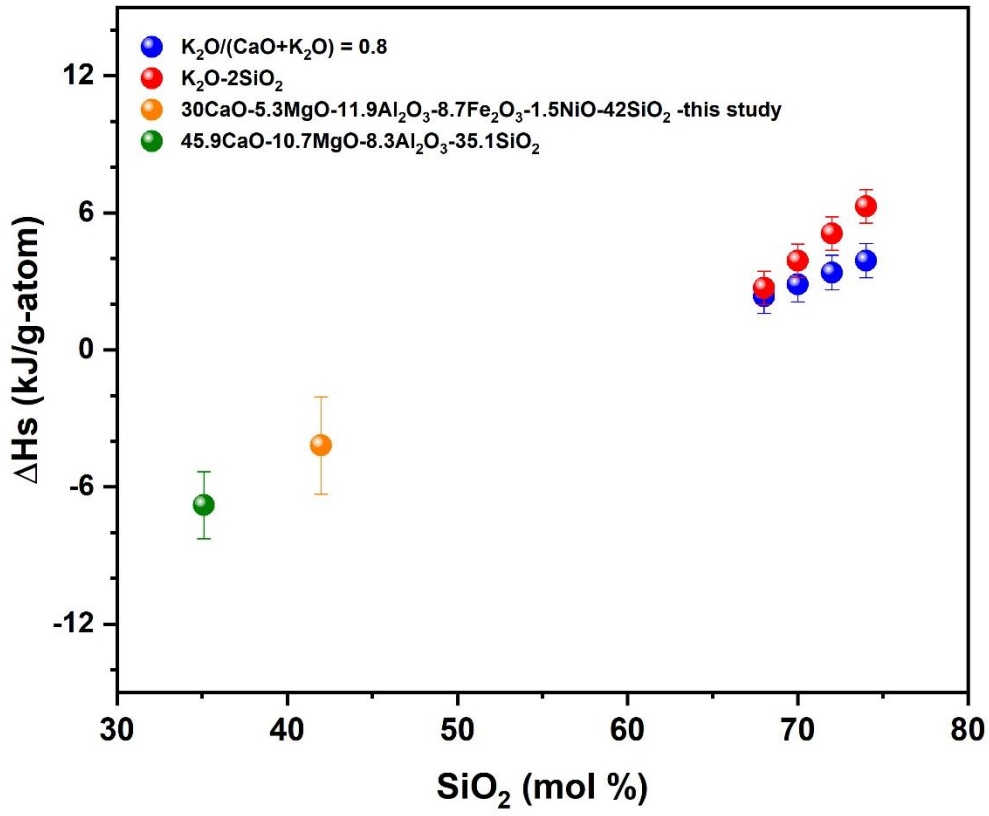

Fig. 2 – Enthalpies of solution (ΔH_{sol}) of SiO_2 in silicate melts with varying SiO_2 mole percent. Green,[21] blue,[16]and red[16] spheres are reference values.

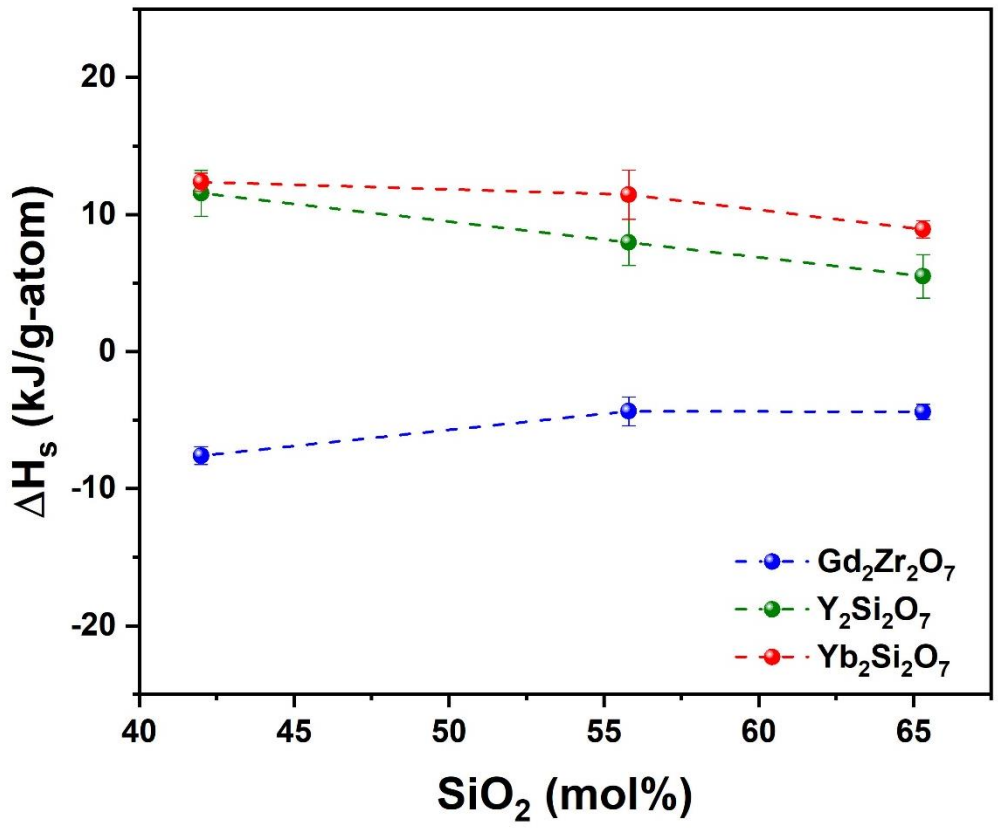

Fig. 3 – Enthalpies of solution (ΔH_s) of the $Gd_2Zr_2O_7$, $Y_2Si_2O_7$, and $Yb_2Si_2O_7$ coating materials versus SiO_2 mole percent in CMAS melt.

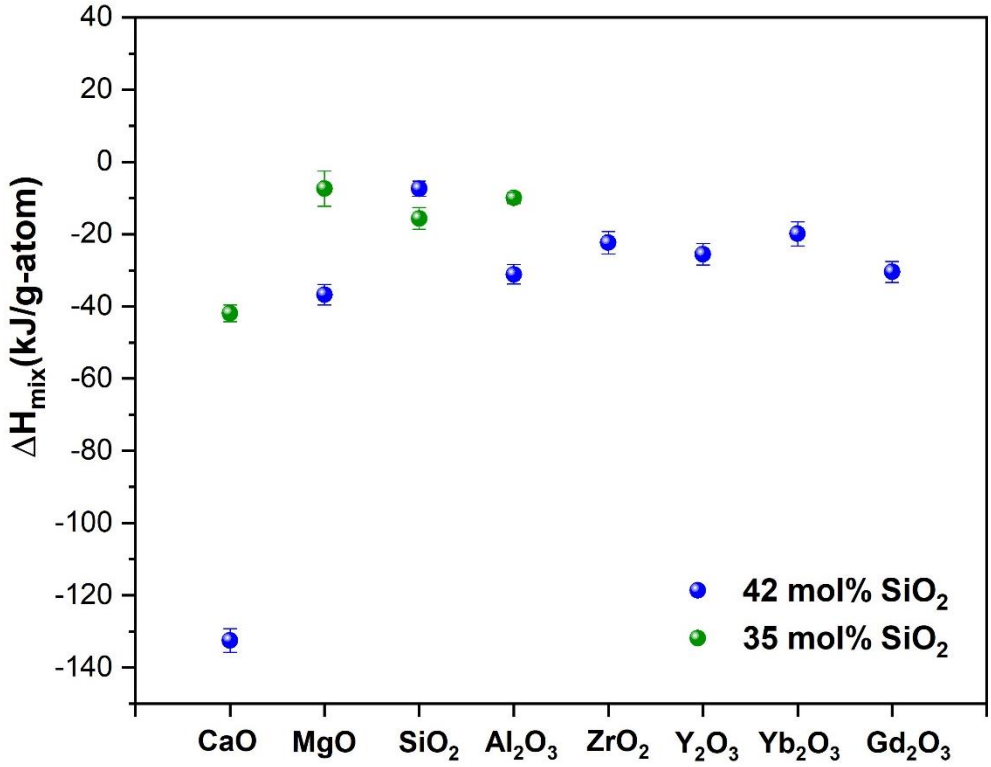

Fig. 4 – Enthalpies of mixing (ΔH_{mix}) of binary oxides in CMAS melts with 35 and 42 mole% SiO_2 (green and blue circles, respectively).

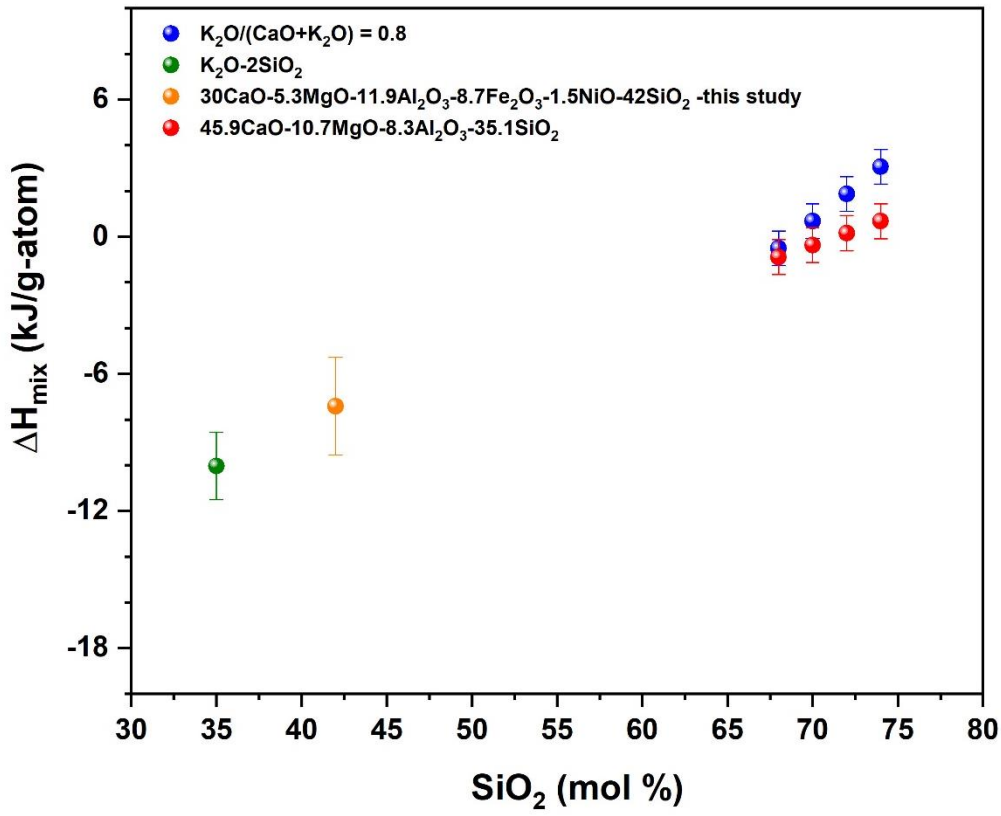

Fig. 5 – Enthalpies of mixing (ΔH_{mix}) of SiO_2 in silicate melts with varying SiO_2 mole percent. Green,[21] blue,[16]and red[16] spheres are calculated from reference ΔH_{sol} values.

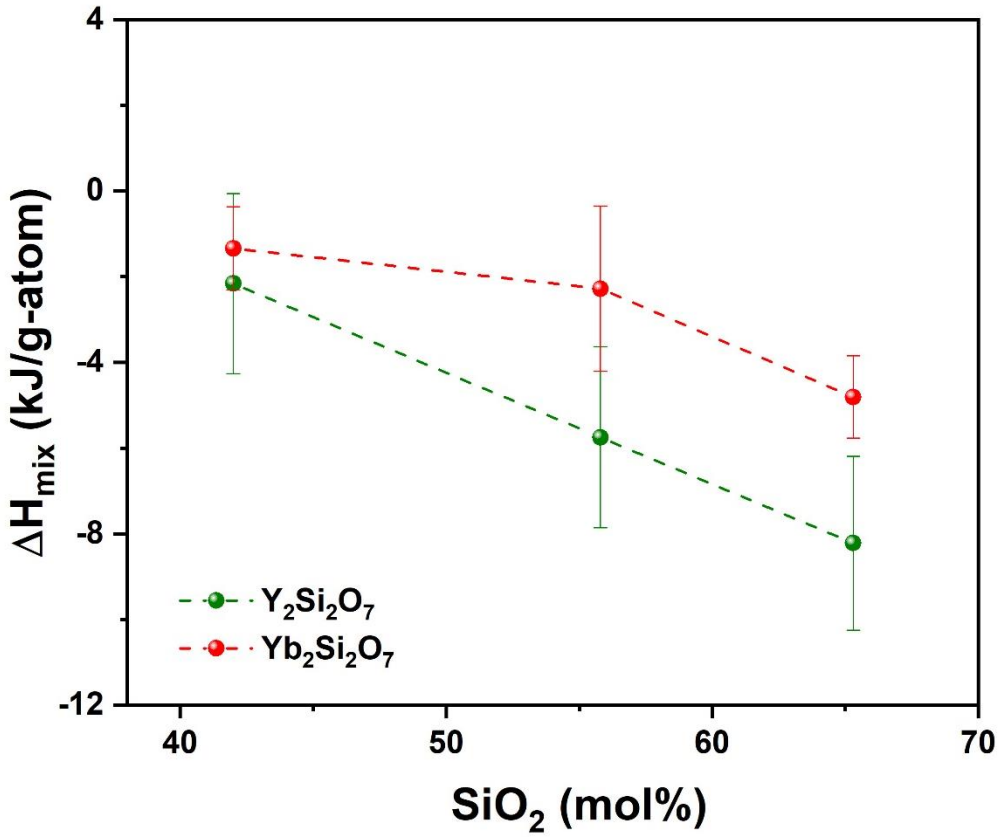

Fig. 6 – Enthalpies of mixing (ΔH_{mix}) of the $Y_2Si_2O_7$ and $Yb_2Si_2O_7$ coating materials in CMAS melts versus SiO_2 mole percent.